2019

Improved Performance of Ballasted Tracks under Impact Loading by Recycled Rubber Mats

Ngoc Trung Ngo
University of Wollongong, trung@uow.edu.au

Buddhima Indraratna
University of Wollongong, indra@uow.edu.au

Cholachat Rujikiatkamjorn
University of Wollongong, cholacha@uow.edu.au

Improved Performance of Ballasted Tracks under Impact Loading by Recycled Rubber Mats

Abstract

Ballasted tracks at transition locations such as approaches to bridges and road crossings experience increasing degradation and deformation due to dynamic and high impact forces, a key factor that decreases the stability and longevity of railroads. One solution to minimise ballast degradation at the transition zones is using rubber energy absorbing drainage sheets (READS) manufactured from recycled tyres. When placed beneath the ballast layer, READS distributes the load over wider area and attenuate of the load over a longer duration thus decreasing maximum stress, apart from reducing the energy transferred to the ballast and other substructure components. Subsequently, the track substructure experiences less plastic deformation and degradation. These mats also provide an environmentally friendly and cost-effective alternative. In this study, a series of large-scale drop hammer impact tests was carried out to investigate how effectively the READS could attenuate impact loads and help mitigate ballast deformation and degradation. Soft and stiff subgrade were used to investigate the load-deformation response of ballast (with and without READS), subjected to impact loads from a hammer dropped from various heights (hd =100 - 250 mm). Laboratory test results show that the inclusion of READS helps to reduce the dynamic impact load transferred to the ballast layer resulting in significantly less permanent deformation and degradation of ballast, apart from significant attenuation of load magnitude and vibration to the underlying subgrade layers.

Keywords

recycled, loading, impact, under, tracks, mats, ballasted, rubber, performance, improved

Disciplines

Engineering | Science and Technology Studies

Publication Details

Ngo, T. Ngoc ., Indraratna, B. & Rujikiatkamjorn, C. (2019). Improved Performance of Ballasted Tracks under Impact Loading by Recycled Rubber Mats. Transportation Geotechnics, 20 100239-1-100239-16.

Improved Performance of Ballasted Tracks under Impact Loading by Recycled Rubber Mats

Trung Ngoc Ngo, PhD, MIEAust.

Research Fellow, Centre for Geomechanics and Railway Engineering (CGRE) and ARC Training Centre for Advanced Technologies in Rail Track Infrastructure (ITTC-Rail), University of Wollongong Australia, Wollongong, NSW 2522, Australia.

Buddhima Indraratna, PhD (Alberta), FIEAust., FTSE, FASCE

Distinguished Professor of Civil Engineering, Research Director, Centre for Geomechanics and Railway Engineering (CGRE) and ARC Training Centre for Advanced Technologies in Rail Track Infrastructure (ITTC-Rail), University of Wollongong Australia, Wollongong, NSW 2522, Australia.

Cholachat Rujikiatkamjorn, PhD, FIEAust.

Associate Professor, Centre for Geomechanics and Railway Engineering (CGRE) and ARC Training Centre for Advanced Technologies in Rail Track Infrastructure (ITTC-Rail), University of Wollongong Australia, Wollongong, NSW 2522, Australia.

Technical paper submitted to: **Transportation Geotechnics**

Author for correspondence:

Distinguished Professor Buddhima Indraratna

Faculty of Engineering and Information Sciences

University of Wollongong Australia

Wollongong, NSW 2522

Australia.

Ph: +61 2 4221 3046

Fax: +61 2 4221 3238

Email: indra@uow.edu.au

Improved Performance of Ballasted Tracks under Impact Loading by Recycled Rubber Mats

Trung Ngoc Ngo[1] MIEAust, Buddhima Indraratna[2] F.ASCE and Cholachat Rujikiatkamjorn[3]

[1]Research Fellow, Centre for Geomechanics and Railway Engineering (CGRE), ARC Training Centre for Advanced Technologies in Rail Track Infrastructure (ITTC-Rail), University of Wollongong Australia, Wollongong, NSW 2522, Australia.
Email: trung@uow.edu.au, Ph: +61 2 4221 3385 Fax: +61 2 4221 3238

[2]Distinguished Professor of Civil Engineering, Research Director, Centre for Geomechanics and Railway Engineering (CGRE), ARC Training Centre for Advanced Technologies in Rail Track Infrastructure (ITTC-Rail), University of Wollongong Australia, Wollongong, NSW 2522, Australia.
Email: indra@uow.edu.au, Ph: +61 2 4221 3046 Fax: +61 2 4221 3238

[3]Associate Professor, Centre for Geomechanics and Railway Engineering (CGRE), ARC Training Centre for Advanced Technologies in Rail Track Infrastructure (ITTC-Rail), University of Wollongong Australia, Wollongong, NSW 2522, Australia.
Email: cholacha@uow.edu.au, Ph: +61 2 4221 5852 Fax: +61 2 4221 3238

ABSTRACT: Ballasted tracks at transition locations such as approaches to bridges and road crossings experience increasing degradation and deformation due to dynamic and high impact forces, a key factor that decreases the stability and longevity of railroads. One solution to minimise ballast degradation at the transition zones is using rubber energy absorbing drainage sheets (READS) manufactured from recycled tyres. When placed beneath the ballast layer, READS distributes the load over wider area and attenuate of the load over a longer duration thus decreasing maximum stress, apart from reducing the energy transferred to the ballast and other substructure components. Subsequently, the track substructure experiences less plastic deformation and degradation. These mats also provide an environmentally friendly and cost-effective alternative. In this study, a series of large-scale drop hammer impact tests was carried out to investigate how effectively the READS could attenuate impact loads and help mitigate ballast deformation and degradation. Soft and stiff subgrade were used to investigate the load-deformation response of ballast (with and without READS), subjected to impact loads from a hammer dropped from various heights (h_d =100 - 250 mm). Laboratory test results show that the inclusion of READS helps to reduce the dynamic impact load transferred to the ballast layer resulting in significantly less permanent deformation and degradation of ballast, apart from significant attenuation of load magnitude and vibration to the underlying subgrade layers.

Keywords: Ballast, Rail transport, Recycled rubber mats, Impact loading, Particle breakage, Load attenuation, Stress transfer

1. Introduction

Ballasted rail tracks are the major infrastructure for freight and passenger transport in Australia; this rail network is more than 40,000 km long and provides a vital supply chain to the agriculture and mining industries (Indraratna *et al.* 2011a). Australian rail infrastructure is often constructed on coastal subgrade soils that can lead to excessive settlements and unstable track conditions. In recent years traditional railway foundations have become overloaded due to increasing demand for faster and heavier trains. This demand is accelerating the deterioration of track substructure while increasing the maintenance costs (Selig and Waters 1994, Tutumluer *et al.* 2012, Indraratna *et al* 2014, Boler *et al*. 2018). During operation, rail vehicles generate noise, vibration, and impact loads due to roughness and imperfections at the wheel-rail interface. Impact loads are commonly generated by: (i) differential stiffness at track transition zones such as bridge approaches, rail crossings, and turnouts; and (ii) rail abnormalities such as wheel flats and dipped rails which seriously hamper the safety and efficiency of tracks (Varandas *et al.* 2011, Insa *et al.* 2014). It is also noted that track transitions such as bridge approaches, road crossings and slab tracks in connection with ballasted tracks are common locations of accelerated track degradation due to abrupt changes in support stiffness, and associated differential settlements. Differential settlement contributes to gaps forming just beneath sleepers, hence the effective support stiffness can decrease greatly as felt by carriages.

During passage of trains, ballast aggregates spread laterally mainly due to inadequate confining pressure and they deteriorate as angular corners and sharp edges break (Indraratna *et al.* 2016, Powrie et al. 2007, Sayeed and Shahin 2016, Le Pen and Powrie 2011). Consequently, ballast becomes fouled, less angular and has reduced shear strength, which leads to enforced speed restrictions and more frequent track maintenance. A large proportion of track maintenance costs is related to issues with track substructure such as ballast degradation, fouling, poor drainage (mud-pumping), differential settlement, and track buckling (Tennakoon *et al.* 2012, Navaratnarajah *et al*. 2018, Ngo *et al.* 2017a). In NSW alone, replenishing ballast costs over $15 million per year and it has a detrimental impact on the landscape and environment. In the USA the annual cost of maintenance for ballast tamping and surface alignment is approximately $3,800 per kilometre (Chrismer and Davis 2000). Hence, there is a definite need for innovative design solutions that can minimise ballast degradation and extend the service life of tracks to cater for faster and heavier trains.

Previous studies showed that planar polymeric geogrids could improve track stability and facilitate track drainage through the interaction between ballast particles and apertures (Bathurst and Raymond 1987, Kwon and Penman 2009, Indraratna *et al.* 2011b). The ability of geogrid reinforcement to provide lateral constraint to ballast has been discussed by McDowell *et al*. (2006), Shukla and Yin (2006), Ngo *et al.* (2016). The effect of placing geogrid under ballast lying on stiff foundation (e.g. under concrete bridge decks or level crossings) or at transition zones may be limited because it may not adequately absorb the predominant impact loads (Nimbalkar and Indraratna 2016, Ngo *et al.* 2017b). In fact despite the use of geogrid, significant ballast degradation has been observed and measured in the field by Indraratna *et al.* (2014).

The use of resilient rubber mats in rail tracks to reduce noise and vibration has become increasingly common (e.g. Auersch 2006, Hanson and Singleton 2006, Wettschureck 1997). Rubber mats have recently been trialled for track substructure under stiff foundations to minimise permanent deformation and degradation of aggregates, while enhancing the overall track stability (Costa *et al*. 2012, Lakuši *et al*. 2010, Finegan and Gibson 1999). These studies found that the rubber mats could provide better load transfer at the interface between ballast aggregates and stiff foundation by increasing the contact area, reducing the contact forces, thus minimising track damage.

Most of these previous studies have been conducted either in controlled laboratory or field trial tests subjected to limited loading and boundary conditions; a few attempts have been made to study the effects of rubber mats under high dynamic impact loads. Given that installing rubber mats in rail tracks helps to absorb energy, attenuates impact loads and reduces track vibration, the actual interaction mechanisms between the ballast and rubber mats are complex, depending on the type of inclusions, the nature of the subgrade, and the stress state in the track environment. Moreover, studies on the performance of rubber mats under different subgrade conditions while being subjected to varying magnitudes of impact loads are limited. Müller (2008) confirmed that when rubber mats were installed in stiff foundations, they performed differently than when placed on soft subgrade.

This paper presents a study on how READS influence in mitigating ballast breakage and reducing ballast deformation by conducting a series of large-scale impact tests on ballast. The idea of the testing program in this study was to demonstrate how the rubber mats can be effectively used to decrease the deformation and degradation (breakage) of ballast under impact loads. To the authors'

knowledge, the mechanism of improvement of a recycled rubber mat when placed underneath the ballast is a combination of: (i) attenuation of the load over a longer duration thus reducing the peak; (ii) distributing the load over wider area thus decreasing the maximum stress; and (iii) the absorption of the energy imparted by impact loads that could then reduce the amount of energy transferred to the ballast layer.

2. Experimental study

2.1. Drop weight impact testing facility

A high-capacity drop weight impact testing equipment was used to evaluate the ability of READS to attenuate dynamic impact loads and mitigate ballast degradation (Figure 1a). The impact apparatus consists of a 5.81 kN free fall hammer that can be dropped from a maximum height of 6 m, with an equivalent maximum drop velocity of 10 m/s (Remennikov and Kaewunruen 2010). The hammer is attached to rollers that are guided through low-friction runners on vertical steel columns fixed onto a reinforced concrete floor. A schematic diagram of a typical ballast sample tested in the laboratory is shown in Figure 1b. It is noted that the thickness of subgrade can influence the test results. Given the fixed dimensions of the steel mould and the surrounding cell membrane (approx. 600 mm height), the thickness of ballast and capping layers have been maintained to be 350 and 100 mm, respectively, to represent typical Australian track conditions, and also a 50mm thick subgrade layer was placed within the depth limitation of the test chamber.

A piezoelectric accelerometer was attached to the top surface of the sample assembly to measure acceleration. The accelerometer was positioned at a distance of 42 mm away from the center of the specimen, as shown in Figure 1b. A dynamic load cell was attached to the hammer to record the impact loads during testing, and a high speed camera (recording at 500 frames per second) was used to record the deformation during testing (Figure 1c). These instruments were connected to a host computer controlled data acquisition system (Figure 1d). The drop hammer was hoisted mechanically to the required height and was released by an electronic control system. During the tests, the impact load and acceleration were recorded digitally and filtered using a low-pass fourth-order Butterworth filter with a cut-off frequency of 2,000 Hz.

159 It is worth mentioning that typical Australian heavy haul and freight trains can have a length of up
160 to 5 km long. These trains will generate multiple repeated impact loads due to roughness and
161 imperfections at the wheel-rail interface or when they pass through transition zones such as bridge
162 approaches, rail crossings, etc. In the absence of appropriate laboratory facilities to simulate actual
163 impact of a very long train running on ballast track, the repeated hammer dropping test (impact
164 testing facility) is considered as an appropriate test to characterize ballast performance with
165 different track substructure components (soft and stiff subgrade). The impact testing facility was
166 designed and built at the University of Wollongong Australia, has been widely used to test railway
167 concrete sleepers by Remennikov and Kaewunruen (2010) subjected to high impact loading, and
168 routinely used by railway asset owners in the state of NSW for testing track elements.

169

170 *2.2. Materials tested*

171 All tests were conducted on a simulated track substructure lying on: (a) soft subgrade, and (b) stiff
172 subgrade (reinforced concrete base) to represent a bridge. Ballast aggregates taken from Bombo
173 quarry near Wollongong city is latite basalt, an igneous rock form commonly found along the south
174 coast of New South Wales, Australia. These dark aggregates have a high compressive strength and
175 sharp angular corners when blasted and quarried. Uniaxial compressive strength of parent rock
176 used for ballast aggregates is approximately, σ_c =130 MPa. The ballast has been sieved, cleaned,
177 weighed, and mixed according to the current Australian practices (AS:2758.7, 2015), shown in
178 Figure 2. A 50 mm thick layer of sandy-clay soil, compacted at 7% moisture content to a bulk unit
179 weight of 18.5 kN/m^3, was placed at the bottom of the apparatus, and then a 100 mm thick layer
180 of capping (sub-ballast) consisting of a sand and gravel mixture (Figure 3a) compacted to a bulk
181 unit weight of 20.5 kN/m^3 was placed on top of the subgrade layer. The capping layer was replaced
182 by a reinforced concrete base to simulate a stiff foundation (i.e. crossings or concrete bridge decks).
183 A recycled rubber mat, manufactured from a recycling company in Australia, was placed on top
184 of the capping layer (Figure 3b), followed by a 350 mm thick layer of ballast. Total weight of
185 ballast (38.3 kg) was used for each test and was divided and compacted into 3 equal sub-layers
186 (i.e. 115 mm thick). The ballast aggregates in each sub-layer were painted in different colours to
187 help assess the amount of degradation each layer experiences during the tests, i.e. yellow for the
188 bottom layer, no colour for the middle layer, and red for the top layer (Figure 3c-d). A rubber pad

was attached to the vibrator to prevent particle breakage during tamping. A recycled energy absorbing drainage mat (READS) contain very small perforations to facilitate drainage and to prevent build-up of interface water pressures. These perforations also act as 'frictional' elements maintaining good contact with the granular layer on either side (ballast and sub-ballast). Essentially, this mat is permeable and it has a permeability coefficient approximately of 2.5×10^{-4} cm/sec. It is worth mentioning that upon repeated train loading, fine particles may accumulate on the surface of the mat, and as a result the permeability may be decreased, as observed in a field trial in Singleton (Indraratna et al. 2014). The mechanical properties of the READS used in the laboratory are presented in Table 1.

Dynamic impact loads are commonly caused by wheel or rail abnormalities such as flat wheels, dipped rails, expansion gaps between two rail segments, imperfect rail welds and rail corrugations, and transition zones (Esveld 2001, LePen 2008, Priest *et al.* 2010). The flange-way gap that provides clearance between the wheel flange and the point where rails intersect is also responsible for the development of large impact loads (Anastasopoulos *et al.* 2009). When a train passes through a rail crossing and through turnouts or transition zones, the rapid change in wheel rail contacts coupled with sudden variations in track stiffness causes the wheels to displace up and down, giving rise to impact loads (Paixão *et al.* 2014, Remennikov and Kaewunruen 2014, Powrie *et al*. 2007). Impacts at turnouts may also occur at the switch points due to the shape and flexibility of the movable blades used to control the direction of train passage (Bruni *et al*. 2009). At transition points such as bridge approaches, road crossings and slab track to ballasted track, a considerable change in track stiffness causes high impact forces that accelerate track deformation. This issue becomes even more critical for shared lines between faster passenger trains and heavier freight trains.

2.3. Sample preparation and testing program

A 7 mm thick cylindrical rubber membrane having a 300mm diameter was used to assemble the ballast specimen (Figure 4a). Two halves of a steel mould that surrounds the cell membrane (Figure 4b) were used to support the sample during the compaction. The capping material (sub-ballast) was also weighed, sieved, and compacted to a thickness of 100 mm following the particle size distribution described in Figure 2. A layer of recycled rubber mat (READS -10mm thick) was placed above the capping layer.

219 The first layer of ballast was placed directly onto the READS and was compacted using a hand-
220 held vibrating hammer to attain a unit weight of 15.5 kN/m^3. This process was repeated for the
221 next two layers of ballast (Figure 4c), and then a steel plate (loading plate) was fitted at the top of
222 the ballast and fastened by steel ties. The initial height of specimen was measured and recorded at
223 four evenly spaced points around the cell. The circumference of the cell was measured at three
224 locations (i.e. bottom layer, middle layer, and the top layer of ballast). These initial measurements
225 serve as references for determining the vertical and lateral deformation of the ballast assembly as
226 the tests progress. It is noted that the use of a membrane to confine ballast does not perfectly
227 represent the actual field conditions where the aggregates displace laterally under limited lateral
228 confinement provided by sleepers and ballast shoulders (Indraratna *et al.* 2011a). A 7 mm thick
229 cylindrical rubber membrane could include some boundary effects to the ballast grains near the
230 walls and may affect the reflection of waves at the boundary, and this boundary influence is a
231 limitation of the equipment. A rigid boundary with low friction (i.e. cylindrical steel tube) was
232 also tried but it generated a large impulse shock and the ballast assembly vibrated significantly
233 when the hammer dropped onto to the sample, hence not suitable for assembling ballast specimens.
234 Therefore, the use of a 7 mm thick cylindrical rubber membrane is the most suitable for the impact
235 test and the boundary condition have been maintained constantly for all the tests. An additional
236 confining stress induced on the ballast specimen by the membrane ($\Delta\sigma_3$) at a given number for
237 hammer drops can be estimated and described in Appendix 1.

238 A total of 16 tests were conducted on ballast with and without the inclusion of READS placed on
239 a soft subgrade (Young's modulus of elasticity of subgrade, E_{su} = 55MPa) and a stiff base
240 (concrete) subjected to varying impact loads (i.e. varying drop heights of the hammer as: h_d = 100
241 mm, 150 mm, 200 mm and 250mm), as shown in Figure 4e. These drop heights produce equivalent
242 dynamic stresses between 250-550 kPa, simulating typical impact forces caused by wheel flats and
243 dipped rail joints in the field (Jenkins, et al. 1974, Esveld 2001, Indraratna *et al*. 2011a). A
244 previously made reinforced cylindrical concrete base (300 mm in diameter and 100 mm in
245 thickness) was used as the stiff base, which was placed directly on the subgrade layer. The impact
246 test program is summarised in Table 2. Every test was subjected to 15 drops; after each drop the
247 vertical and lateral displacements of the ballast specimen were measured (Figure 4f). After each
248 test, ballast aggregates in each layer were separately sieved to quantify the amount of breakage.

3. Results and Discussion

3.1. Measured vertical displacement

Figure 5 shows typical images captured by the high speed camera of deformed ballast assemblies, recorded before and after the 10th drop (drop height, h_d = 150 mm). When a hammer was dropped on the top loading plate, it began to compress the ballast specimen (Figure 5a). The sample was compressed to its maximum vertical displacement at time t = 15 ms (Figure 5b), and then the ballast assembly rebounded upwards to a residual position (Figure 5c). Upon impact loading, elastic settlement occurs, followed by plastic vertical displacement. Typical time-settlement responses of ballast assemblies measured at different drops placed on the concrete base, subjected to a drop height of h_d = 150 mm are shown in Figure 6. It is seen that the ballast assemblies deform from their original position to a maximum displacement and then return to a residual (permanent) settlement in about 120 ms. The inclusion of READS at the interface of the ballast/capping layer resulted in decreased deformation of ballast. The maximum vertical displacement after the 15th drop, with and without the inclusion of READS, is 77.05 mm and 84.76 mm, respectively, and the corresponding residual settlement is 64.50 mm and 74.20 mm. It is noted that the presence of the mat increases the elastic range of movement before plastic deformation of the ballast can take place, and moreover by attenuating the peaks in the loading to reduce the plastic deformation (Figure 6). The presence of a rubber layer beneath the ballast layer is also helpful for stabilising the ballast contacts and improving the homogeneity of stress transfer.

Variation of the peak and residual vertical displacements of a ballast assembly placed on stiff subgrade and subjected to a given drop height of h_d = 150 mm is plotted in Figure 7. As expected, the vertical displacement of the ballast specimen without READS is higher than the READS-reinforced ballast assembly. The laboratory test data show that ballast deformation increases with an increase in number of hammer drops due to the reorientation, rearrangement, and corner breakage of aggregates. Towards the end of testing, the deformation of ballast occurs at a diminishing rate.

Figure 8 shows the variations of the accumulated permanent vertical settlement of ballast assemblies with and without READS placed on both soft and stiff subgrade. As expected, settlement generally increases as the drop height, h_d increases. There is a distinct trend of increasing vertical settlement within the first ten impact drops followed by a gradual increase of

vertical displacement at a decreasing rate. After attaining a threshold compression after the 10th drop, the ballast resists further settlement, but promotes particle breakage.

3.2. Measured lateral deformation

Under an impact load, ballast aggregates are compressed and displaced laterally. After each hammer drop, the circumference of ballast specimens was measured at the top, middle, and bottom of the ballast layers (locations: A, B, C in Figure 5a). The average accumulative lateral displacements, S_h for each test are shown in Figure 9. Measured data indicate that in every case the lateral deformation increases with successive impacts, but the rate of increase in lateral deformation gradually reduces after the 10th drop. The initially rapid lateral displacement of ballast could be attributed to the high rate of ballast degradation that takes place at this stage. Indraratna *et al*. (2013) observed that ballast deformation was mainly due to the breakage of ballast particles and particle re-arrangement. With the inclusion of READS, measured lateral deformation of ballast decreases for both types of subgrade because the energy absorbing capacity of READS ensures less energy to be transferred to ballast aggregates and thereby reduce deformation. It is seen from Figs. 8 and 9 that the recycled rubber mat provides beneficial effects in decreasing the vertical and lateral deformation of ballast assemblies when placed on both soft and stiff (concrete) subgrades. Compared to a stiff subgrade, a weak subgrade itself serves as a flexible cushion to attenuate the impulse waves; hence, the beneficial role of the ballast mat remains under-utilized (i.e. less reduction in ballast deformation). The effect of subgrade stiffness is best interpreted and further discussed based on Figure 12.

3.3. Ballast breakage

Impact loads produce a series of physical phenomena such as elastic shock, plastic wave propagation, fracture and fragmentation that affects the strength and deformation of granular materials (Meyers 1994). After the impact tests, different types of particle degradation were observed such as grinding (abrasion), angular corner breakage (due to attrition), and distinct splitting across the body of particles (fracture). The ballast breakage index (*BBI*) was first introduced by Indraratna *et al*. (2005) based on the particle size distribution (PSD) curves, and it has been widely used to quantify ballast breakage. The *BBI* is determined on the basis of change in the fraction passing a range of sieves, where the amount of ballast breakage causes the PSD curve to shift further towards the smaller particles size region on a conventional PSD plot, as

described in Figure 10. The *BBI* is given by the relationship: *BBI=A/(A+B)*, where, *A* is shift in the PSD curve after the load application and *B* is potential breakage or the area between the arbitrary boundary of maximum breakage and the final PSD curve. The *BBI* with and without the inclusion of READS placed on the soft and stiff subgrade, subjected to varying drop heights (h_d = 100-250 mm) are plotted in Figure 11. As expected, the maximum ballast breakage occurs in the top layer, and it decreases in the middle and bottom layers as the induced impact loads attenuate with depth. Figure 11 shows a large increase in ballast breakage when the drop height of the hammer increases (increased impact energy); this agrees with the findings of a previous study using a large-scale triaxial apparatus where ballast breakage was observed to increase with an increase in cyclic loads (Sun *et al*. 2018).

The highest value of *BBI*=0.352 was obtained for test CN250 where ballast was placed on stiff subgrade (without READS), and the lowest breakage (*BBI* =0.077) was measured for the test SY100 (placed on soft subgrade with READS). When placed on stiff subgrade, it was observed that ballast at the bottom layer still experienced considerable breakage, unlike the ballast in the middle layer which experienced the least (Figure 11c). This is possibly because the ballast aggregates at the bottom layer are restrained against downward movement by the rigid concrete base, whereas the aggregates in the middle layer are relatively free to displace and rotate due to the underlying flexible ballast layer.

The measured data is best interpreted by Figure 12, which plots the final values of ballast deformation (Figure 12a-d), the percentage reduction of ballast breakage (R_b), and the relative deformation factors (R_v, R_h) with varying drop heights (Figure 12e-f). The relative deformation factors for vertical (R_v) and horizontal displacement (R_h) are defined as follows:

Vertical settlement (%): $$R_v = \frac{S_{v(No\ READS)} - S_{v(With\ READS)}}{S_{v(No\ READS)}} \times 100 \quad (1)$$

Lateral deformation (%): $$R_h = \frac{S_{h(No\ READS)} - S_{h(With\ READS)}}{S_{h(No\ READS)}} \times 100 \quad (2)$$

Reduction in breakage (%): $$R_b = \frac{BBI_{No\ READS} - BBI_{With\ READS}}{BBI_{No\ READS}} \times 100 \quad (3)$$

It is seen that the vertical and lateral deformations with READS are less than those without READS for a given drop height. The beneficial effects of READS are more pronounced on the stiff

subgrade, and this corroborates with the energy absorbing nature of READS whereby less energy is transferred to the ballast and other substructure components, thus reduced deformation and degradation. The effect of READS is reflected by reduction factors presented in Figure 12e-f. It is seen that READS could decrease the deformation of ballast around 7-15% for a given drop height. The reduction in breakage, R_b was measured up to 28% (stiff subgrade) while R_b fluctuated around 10 to 17% for the soft subgrade (average for three layers).

3.4. Measured impact forces

Figure 13 shows the impact forces measured with and without READS placed on soft subgrade and subject to varied drop heights, h_d = 100-250 mm. Data was recorded during the first 200 milliseconds (ms) and was measured at the 10th drop (N=10). Subject to a free-fall hammer, multiple P_1 type peaks occur followed by the distinct P_2 type peak. It is noted that all tests have a similar response pattern with multiple peak forces (P_1) followed by another peak of smaller magnitude (the so-called P_2 force). An instantaneous sharp peak with very high frequency known as P_1, and a gradual peak of smaller magnitude and with a relatively lesser frequency, known as P_2. The impact force P_1 comes from the inertia of the rail and sleepers that resist the downward motion of the wheel, and this leads to compression in the contact zone between the wheel and the rail. The force P_2 prevails over a longer duration and is attributed to the mechanical resistance of the track substructure leading to significant compression. P_2 directly causes ballast breakage and it can be estimated based on the mathematical model proposed by Jenkins *et al*. (1974):

$$P_2 = P_0 + 2\alpha V \times \left[\frac{M_u}{M_u+M_t}\right]^{0.5} \times \left[1 - \frac{C_t\pi}{4[K_t(M_u+M_t)]^{0.5}}\right] \times [K_t M_u]^{0.5} \quad (4)$$

where, P_0: static wheel load (kN); M_u: vehicle unsprung mass (kg); 2α is the total joint dip angle (rad); V: train speed (m/s); K_t: equivalent track stiffness (MN/m); C_t: equivalent track damping (kNs/m); and M_t: is the equivalent track mass (kg).

The first peak has a sharp triangular shape and a high amplitude between 160 kN to 375 kN for h_d =100-250 mm within relatively short time duration (about 15 ms). The second peak was measured approximately 20 ms after the first peak, followed by several local triangular shaped peaks of around 40 kN (about 100 ms from the first peak). Remennikov and Kaewunruen (2010) found that the inertial force peak induces the specimen to vibrate during the first 15 ms. Any further vibration could separate the hammer and the ballast specimen, as shown by a sharp reduction in the impact

force to almost zero for a short period of 10-30 ms (after the first P_1 force). The deformation of the ballast assembly continues to rapidly absorb the additional kinetic energy of the impactor but with smaller impact forces. This process repeated itself several times until the impact load remained at a stable value of around 40 kN (P_2 force).

Figure 14 illustrates the overlaying plot of impact forces onto the plot of measured vertical displacements to identify where along the displacement plot in each scenario the peak P_1 force occurs for a soft subgrade soil for h_d=100mm. It is seen that the P_1 occurs within the first 40 ms during the impact where a significant elastic deformation of ballast occurs. Figure 15 shows comparison of the maximum impact forces P_1 and P_2 after the 15th drop for soft and stiff subgrades. The magnitude of impact force P_1 varies from 154 kN to 500 kN with a short duration of 1 to 15 ms, while the P_2 forces vary from 32 kN to 98 kN. Ballast on stiff subgrade experiences higher maximum impact forces P_1, P_2 than ballast on the soft subgrade; this results in a higher deformation as shown in Figure 12. The inclusion of READS substantially reduces the magnitude of the P_1 and P_2 impact force.

3.5. Measured acceleration responses

Typical acceleration of ballast under soft and stiff subgrade (with and without READS) measured at the 10th drop (N=10) subjected to a drop height of h_d = 100 mm is shown in Figure 16. It is noteworthy that the inclusion of recycled rubber mats reduces the peak acceleration and helps to attenuate vibration faster for soft and stiff subgrades. There are several peaks that corroborate with P_1 force, as shown in the impact force-time plots, and the acceleration becomes negligible after 100 ms. When the hammer first hits the specimen the maximum force P_1 is observed. With soft subgrade, maximum accelerations are around 66 g and 105 g for the ballast assembly with and without READS, respectively. The accelerations measured approximately 110 g (with READS) and 169 g (without READS) for stiff subgrade. When the P_2 force is reached, the mean acceleration is measured around 12 g and 20 g for soft and stiff subgrade, respectively. Also, the inclusion of READS helps to attenuate vibration faster, as shown in Figure 16b.

Measured accelerations for stiff subgrade are always larger than those for the soft subgrade, which indicates higher levels of vibration at the sleeper-ballast interface. In order to provide further quantitative information related to the energy absorbing characteristics of the recycled rubber mat used in this study, the estimation of energy absorption of the mats based on the strain energy

concept (i.e. based on the measured deformation of ballast specimen) is described in Appendix 2. It is therefore recommended that the use of READS as a promising approach to be considered for transition zones to reduce vibration and prevent excessive ballast deformation and breakage. This can increase safety and passenger comfort due to vibration attenuation, and lead to a more economical track design due to the subsequent reduction in ballast degradation.

4. Conclusions

This paper presented the laboratory results from large-scale impact tests to investigate the role that rubber energy absorbing drainage sheet (READS) could provide by reducing deformation and degradation of railway ballast under varied impact loading conditions. From measured test data, the following salient conclusions can be drawn:

- Test data showed that vertical and lateral deformation of ballast increased with the number of impact blows. These observations were more pronounced during the first ten impact drops due to initial densification and further grain packing caused by particle breakage. But once the ballast began to stabilise, the rate of deformation gradually decreased for the subsequent impact drops. The inclusion of READS attenuated both the axial and lateral deformation of ballast, as well as particle degradation under impact loading.
- Two distinct types of force peaks were measured: multiple instantaneous P_1 peaks followed by a gradual P_2 peaks of smaller magnitude and longer duration. The magnitude of impact force P_1 varied from 154 kN to 500 kN with a short duration of around 15 ms, where the P_2 forces were around 32 kN to 98 kN. Note that the maximum values of P_1 and P_2 forces increased progressively throughout successive impact blows as the ballast assembly became denser, but these peak values decreased when READS were provided below the ballast layer. READS (energy absorption layer) could reduce the dynamic impact that would have otherwise been transmitted into the ballast and underlying sub-layers. Ballast layer placed on stiff subgrade experienced higher maximum impact forces P_1 and P_2 than the one placed on soft subgrade. In addition, laboratory measurements showed that less vibration (acceleration) occurred when READS was installed.

The laboratory results obtained in this study provided a better understanding of the capacity of READS to attenuate and distribute the load over wider area, and thus reduce the deformation and

degradation of ballast. In essence, this study presented a quantitative understanding of the extent that the READS could reduce impact-induced forces in ballast while attenuating vibration, as well as substantially reducing ballast breakage.

5. Acknowledgements

This research was conducted by the Australian Research Council Industrial Transformation Training Centre for Advanced Technologies in Rail Track Infrastructure (IC170100006). The authors also greatly appreciate financial support from the Rail Manufacturing Cooperative Research Centre, with subsequent support from organizations including the Australasian Centre for Rail Innovation (ACRI), Tyre Stewardship Australia (Project R2.5.1). The authors thank to graduate student, Timothy Beckmans for their help during laboratory test. The authors appreciate Tim Neville (ARTC) for encouraging the use of recycled rubber mats in real-life tracks. The authors are also grateful to Alan Grant, Cameron Neilson, and Duncan Best for their assistance during the laboratory work. The authors thank Robert Clayton (English editor) for proofreading and professionally editing the manuscript.

Appendix 1: Estimation of induced lateral confinement provided by the membrane

Subjected to impact loads, the membrane deforms laterally. Additional lateral confinement (i.e. induced lateral confinement, $\Delta\sigma_3$) provided by the membrane can be estimated using the hoop tension theory. Using the Hooke's law, the circumferential stress (σ_c) can be estimated by:

$$\sigma_c = \frac{M_m}{(1+\nu_r)\cdot(1-2\nu_r)} \times [(1-\nu_r)\varepsilon_c + \nu_r(\varepsilon_3 + \varepsilon_z)] \quad (5)$$

where, M_m is mobilised modulus of the membrane; ε_c and ε_3 are circumferential and radial strains, respectively. It is noted that, $\varepsilon_c = k.\varepsilon_3$; and the ratio, *k* can be estimated as 0.42 for rubber. ν_r is the Poisson's ratio of recycled rubber mat ($\nu_r = 0.44$)

The loading plate can move downward inside the membrane and ε_z=0, and the Eq. (5) can then be simplified to:

$$\sigma_c = \frac{M_m}{(1+\nu_r)\cdot(1-2\nu_r)} \times [(1-\nu_r)k\varepsilon_3 + \nu_r\varepsilon_3] \quad (6)$$

Due to symmetry of the cylindrical membrane, the lateral confinement applied by the membrane ($\Delta\sigma_3$) can be calculated as:

$$\Delta\sigma_3 = \frac{2\sigma_c}{D} \quad (7)$$

where, *D* is diameter of equivalent circular area of the membrane.

Substituting Eq. 6 into Eq. 7, gives:

$$\Delta\sigma_3 = \frac{2M_m}{D} \times \frac{(1-\nu_r)k + \nu_r}{(1+\nu_r)\cdot(1-2\nu_r)} \times \varepsilon_3 \quad (8)$$

Based on measured changes in the circumference (i.e. ε_3) of a ballast specimen (Figure 9), the induced confining stresses onto the ballast specimen by the membrane can then be calculated. Figure 17 presents estimated values of $\Delta\sigma_3$ for both soft and stiff subgrade under 2 different drop heights, i.e. h_d =100, 200mm. It is seen that the calculated values of $\Delta\sigma_3$ vary from 10-20 kPa. It is noted that the ASTM D4767-11 recommends the use of a correction factor for rubber membrane stiffness when determining the deviatoric stress in triaxial testing; for ballast assemblies, the required correction for deviator stress is around 10-15 kPa (Lackenby *et al*. 2007, Sun *et al*. 2018).

Appendix 2: Estimation of energy absorption of the mats

As the hammer having a weight of *W* falls from rest at a given height h_d, its gravitational potential energy is converted to kinetic energy. Adopting the principle of energy conservation ($Mgh_d = \frac{1}{2}MV_h^2$), the total kinetic energy (E_K) and velocity of hammer when it hits the ballast specimen can be calculated by:

$$E_K = \frac{1}{2}MV_h^2 \quad \text{and} \quad V_h = \sqrt{2gh_d} \tag{9}$$

The total work done (*W*) by ballast specimen upon the impact load can then be estimated as:

- No rubber mat: $W = \frac{1}{2}MV_h^2 = \sigma_3\delta V_0 + (\sigma_1 - \sigma_3)A\delta s_0$ (10)
- With rubber mat: $W = \frac{1}{2}MV_h^2 = \sigma_3\delta V + (\sigma_1 - \sigma_3)A\delta s + E_{RM}$ (11)

where, σ_1 and σ_3 are the major and minor principal stresses, respectively; δV is the volume change of the specimen; δs is the vertical displacement; *A* is cross-section area of the ballast sample; E_{RM} is the estimated energy absorbed by the mat, and this can be approximately determined by subtracting Eq.11 from Eq.10.

It is noted that for impact tests carried out in this study, σ_1 and σ_3 were not directly measured. For the purpose of simplicity, σ_1 can be estimated from the measured P_2 forces (i.e. applied over a long duration and causing ballast deformation), and σ_3 is estimated as the applied confining stress by the membrane (i.e. 20 kPa as estimated in Appendix 1).

Figure 18 presents the estimated energy absorbing capacity of recycled rubber mat placed on the soft and stiff subgrade after a given number of hammer drops for drop heights of h_d=100, 200 mm. It is seen that the measured E_{RM} of the mat increases with an increase in the number of hammer drops, and the recycled rubber mats perform better when placed on the stiff subgrade.

6. References

AS:2758.7: (2015). Aggregates and rock for engineering purposes, Part 7. Railway Ballast. Standard Australia, SAI Global, Australia.

ASTM (2018). Standard test method for consolidated undrained triaxial compression test for cohesive soils, *ASTM D4767-11*. West Conshohocken, PA: ASTM International.

Anastasopoulos, I., Alfi, S., Gazetas, G., Bruni, S. and Leuven, A.V. (2009). Numerical and experimental assessment of advanced concepts to reduce noise and vibration on urban railway turnouts. *Journal of Transportation Engineering, ASCE,* 135(5), pp: 279-287.

Auersch, L. (2006). Dynamic axle loads on tracks with and without ballast mats: numerical results of three-dimensional vehicle-track-soil models. *Proceedings of the Institution of Mechanical Engineers*, 220(F2), pp: 169-183.

Bathurst, R.J. and Raymond, G.P. (1987). Geogrid reinforcement of ballasted track. *Transportation Research Record,* 1153, pp: 8-14.

Bruni, S., Anastasopoulos, I., Alfi, S., Leuven, V. A., Apostolou, M. And Gazetas, G. (2009). Train-induced vibrations on urban metro and tram turnouts. Journal of Transportation Engineering, ASCE, 135(7), pp.397-405.

Boler, H., Mishra, D., Hou, W. and Tutumluer, E. (2018). Understanding track substructure behavior: Field instrumentation data analysis and development of numerical models. *Transportation Geotechnics*, 17, pp: 109-121.

Costa, P.A., Calçada, R. and Cardoso, A.S. (2012). Ballast mats for the reduction of railway traffic vibrations. Numerical study. *Soil Dynamics and Earthquake Engineering*, 42(0), 137-150.

Chrismer, S., and Davis, D. (2000). Cost comparisons of remedial methods to correct track substructure instability. Transportation Research Record: J Transp. Research Board (1713), 10-14.

Esveld, C. (2001). Modern railway track, MRT Press, The Netherlands.

Finegan, I. C., and Gibson, R. F. (1999). Recent research on enhancement of damping in polymer composites. 542 *Composite Structures*, 44(2–3), 89-98.

Jenkins, H. M., Stephenson, J. E., Clayton, G. A., Moorland, J. W., and Lyon, D. (1974). The effect of track and vehicle parameters on wheel/rail vertical dynamic forces. *Railway Engineering Journal*, 3(1), 2–16.

Hanson, C.E. and Singleton Jr, H.L. (2006). Performance of ballast mats on passenger railroads: Measurement vs. projections. *Journal of Sound and Vibration,* 293(3–5), pp: 873-877.

Indraratna, B., Lackenby, J. and Christie, D. (2005). "Effect of confining pressure on the degradation of ballast under cyclic loading." *Géotechnique,* 55(4), pp: 325-328.

Indraratna, B., Salim, W. and Rujikiatkamjorn, C. (2011a). Advanced Rail Geotechnology - Ballasted Track, CRC Press, Taylor & Francis Group, London, UK

Indraratna, B., Ngo, N.T. and Rujikiatkamjorn, C. (2011b). Behavior of geogrid-reinforced ballast under various levels of fouling. *Geotextiles and Geomembranes,* 29(3), pp: 313-322.

Indraratna, B., Ngo, N.T. and Rujikiatkamjorn, C. (2013). Deformation of coal fouled ballast stabilized with geogrid under cyclic load. *ASCE-Journal of Geotechnical and Geoenvironmental Engineering*, 139(8), pp: 1275-1289.

Indraratna, B., Nimbalkar, S. and Neville, T. (2014). Performance assessment of reinforced ballasted rail track. *Proceedings of the ICE - Ground Improvement*, 167, pp: 24-34.

Indraratna, B., Nimbalkar, S.S., Ngo, N.T. and Neville, T. (2016). Performance improvement of rail track substructure using artificial inclusions – Experimental and numerical studies. *Transportation Geotechnics*, 8, pp: 69-85.

Insa, R., Salvador, P., Inarejos, J. and Medina, L. (2014). Analysis of the performance of under-sleeper pads in high-speed line transition zones. *Proceedings of the Institution of Civil Engineers - Transport*, 167(2), pp: 63-77.

Kwon, J. and Penman, J. (2009). The use of biaxial geogrids for enhancing the performance of sub-ballast and ballast layers-previous experience and research. Bearing Capacity of Road, Railways and Airfields Taylor & Francis Group, London.

Lackenby, J., Indraratna, B., McDowell, G. and Christie, D. (2007). "Effect of confining pressure on ballast degradation and deformation under cyclic triaxial loading." *Géotechnique*, **57**(6), pp: 527-536.

LePen, L. (2008). Track behaviour: the importance of the sleeper to ballast interface. PhD Thesis, University of Southamton, UK.

Le Pen, L.M. and Powrie, W. (2011). Contribution of base, crib, and shoulder ballast to the lateral sliding resistance of railway track: A geotechnical perspective. Proceedings of the Institution of Mechanical Engineers, Part F: *Journal of Rail and Rapid Transit*, 225(2), pp: 113-128.

Lakuši, S., Ahac, M., Haladin, I. (2010) Experimental investigation of railway track with under sleeper pad. Proceedings of the 10th Slovenian Road and Transportation Congress. pp: 386-393.

Remennikov, A.M. and Kaewunruen, S. (2010). Dynamic crack propagation in prestressed concrete sleepers in railway track systems subjected to severe impact loads. *ASCE Journal of Structural Engineering*, 136 (6), pp. 749-754.

Remennikov, A.M. and Kaewunruen, S. (2014). Experimental load rating of aged railway concrete sleepers. *Engineering Structures*, 76, pp: 147-162.

McDowell, G.R., Harireche, O., Konietzky, H., Brown, S.F. and Thom, N.H. (2006). Discrete element modelling of geogrid-reinforced aggregates. *Proceedings of the ICE - Geotechnical Engineering* 159(1), pp: 35-48.

Müller, R. (2008). Mitigation measures for open lines against vibration and ground-borne noise: A Swiss overview. *Noise and Vibration Mitigation for Rail Transportation Systems*, Springer Berlin Heidelberg, 610 264-270.

Navaratnarajah, S.K., Indraratna, B. and Ngo, N.T. (2018). Influence of under sleeper pads on ballast behavior under cyclic loading: experimental and numerical studies. *Journal of Geotechnical and Geoenvironmental Engineering*, 144(9), pp: 04018068.

567 Ngo, N.T., Indraratna, B. and Rujikiatkamjorn, C. (2016). Modelling geogrid-reinforced railway
568 ballast using the discrete element method. *Transportation Geotechnics*, 8(2016), pp: 86-102.

569 Ngo, N.T., Indraratna, B. and Rujikiatkamjorn, C. (2017a). Stabilisation of track substructure with
570 geo-inclusions – experimental evidence and DEM simulation. *International Journal of Rail*
571 *Transportation*.

572 Ngo, N.T., Indraratna, B. and Rujikiatkamjorn, C. (2017b). A study of the geogrid–subballast
573 interface via experimental evaluation and discrete element modelling. *Granular Matter*,
574 19(3), pp: 54: 51-16.

575 Nimbalkar, S. and Indraratna, B. (2016). Improved performance of ballasted rail track using
576 geosynthetics and rubber shockmat. *Journal of Geotechnical and Geoenvironmental*
577 *Engineering*, 142(8), pp: 04016031.

578 Meyers M.A. (1994). Dynamic Behavior of Materials, John Wiley and Sons, Inc. New York.

579 Paixão, A., Alves Ribeiro, C., Pinto, N., Fortunato, E. and Calçada, R. (2014). On the use of under
580 sleeper pads in transition zones at railway underpasses: experimental field testing. *Structure*
581 *and Infrastructure Engineering*, pp: 1-17.

582 Powrie, W., Yang, L.A. and Clayton, C.R.I. (2007). Stress changes in the ground below ballasted
583 railway track during train passage. *Proceedings of the Institution of Mechanical Engineers:*
584 *Part F: Journal of Rail and Rapid Transit*, pp: 247-261.

585 Priest, J.A., Powrie, W., Yang, L., Grabe, P.J. and Clayton, I. (2010). Measurements of transient
586 ground movements below a ballasted railway line. *Géotechnique*, 60(9), pp: 667–677.

587 Selig, E.T. and Waters, J.M. (1994). Track geotechnology and substructure management, Thomas
588 Telford, London.

589 Sayeed, M.A. and Shahin, M.A. (2016). Three-dimensional numerical modelling of ballasted
590 railway track foundations for high-speed trains with special reference to critical speed.
591 *Transportation Geotechnics*, 6, pp: 55-65.

592 Shukla, S.K. and Yin, J.H. (2006). Fundamentals of Geosynthetic Engineering, Taylor & Francis
593 Group, London, UK.

594 Sun, Q., Indraratna, B. and Ngo, N.T. (2018). Effect of increase in load and frequency on the
595 resilience of railway ballast. *Géotechnique*, DOI: https://doi.org/10.1680/jgeot.17.P.302

596 Tennakoon, N., Indraratna, B., Rujikiatkamjorn, C., Nimbalkar, S. and Neville, T. (2012). The role
597 of ballast fouling characteristics on the drainage capacity of rail substructure. *Geotechnical*
598 *Testing Journal*, 35(4), pp: 1-11.

599 Tutumluer, E., Huang, H. and Bian, X. (2012). Geogrid-aggregate interlock mechanism investigated
600 through aggregate imaging-based discrete element modeling approach. *International*
601 *Journal of Geomechanics*, 12(4), pp: 391-398.

602 Varandas, J.N., Hölscher, P. and Silva, M.A.G. (2011). Dynamic behaviour of railway tracks on
603 transitions zones. *Computers & Structures*, 89(13–14), pp: 1468-1479.

604 Wettschureck, R. (1997). Measures to reduce structure-borne noise emissions induced by above-
605 ground, open railway lines. *Rail Engineering International*, Edition, 1, 12-16.

606

607 **List of Tables**

608 Table 1. Mechanical characteristics of READS

Material properties	Values
Thickness, *t* (mm)	10
Area weight, kg/m^2	8.23
Tensile strength, τ (N/mm^2)	0.58
Tensile strain at failure, ε_{ult} (%)	56
Permeability coefficient, *k* (cm/sec)	2.5×10^{-4}
Static bedding modulus, C_{stat} (N/mm^3)	0.142[a]
Dynamic bedding modulus , C_{dyn} (N/mm^3)	0.107[a]

609 [a] DIN (German Institute for Standardization). (2010). "Mechanical vibration—Resilient elements
610 used in railway tracks. Part V: Laboratory test procedures for under-ballast mats." *45673–5*, Berlin.

611

612

613

614 Table 2. Summary of impact testing program

Test no.	Test name	Subgrade condition	READS used	Drop height, h_d (mm)
1	SY100	Soft	Yes	100
2	SN100	Soft	No	100
3	CY100	Concrete	Yes	100
4	CN100	Concrete	No	100
5	SY150	Soft	Yes	150
6	SN150	Soft	No	150
7	CY150	Concrete	Yes	150
8	CN150	Concrete	No	150
9	SY200	Soft	Yes	200
10	SN200	Soft	No	200
11	CY200	Concrete	Yes	200
12	CN200	Concrete	No	200
13	SY250	Soft	Yes	250
14	SN250	Soft	No	250
15	CY250	Concrete	Yes	250
16	CN250	Concrete	No	250

Notation of the test name - for example SY100: S = soft subgrade (C=Concrete / stiff subgrade); Y = with recycled rubber mat; drop height, h_d

615

List of Figures

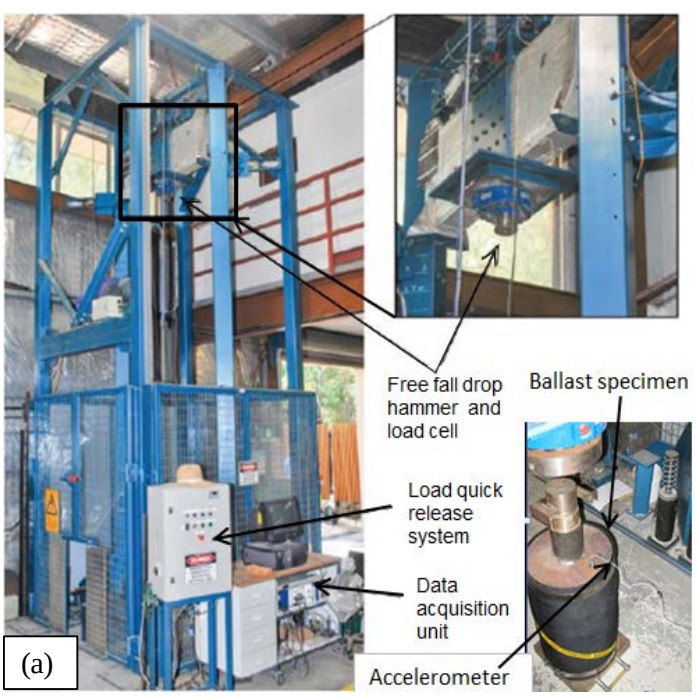

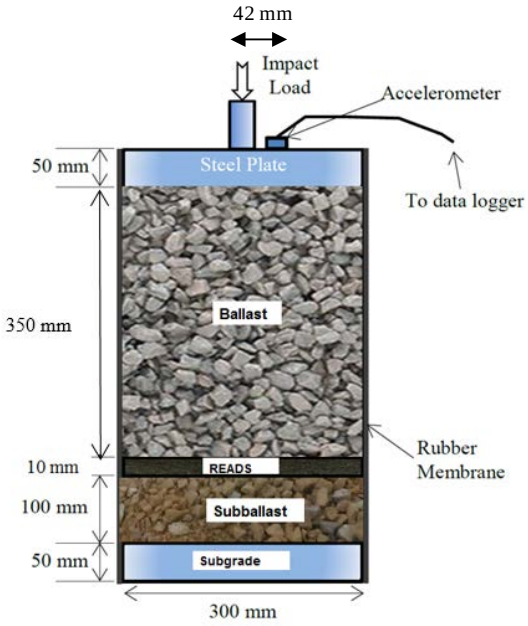

(b)

(c)

(d)

Figure 1. (a) High capacity drop weight impact apparatus; (b) Schematic diagram of ballast sample; (c) High speed camera set up; and (d) Data acquisition unit

622

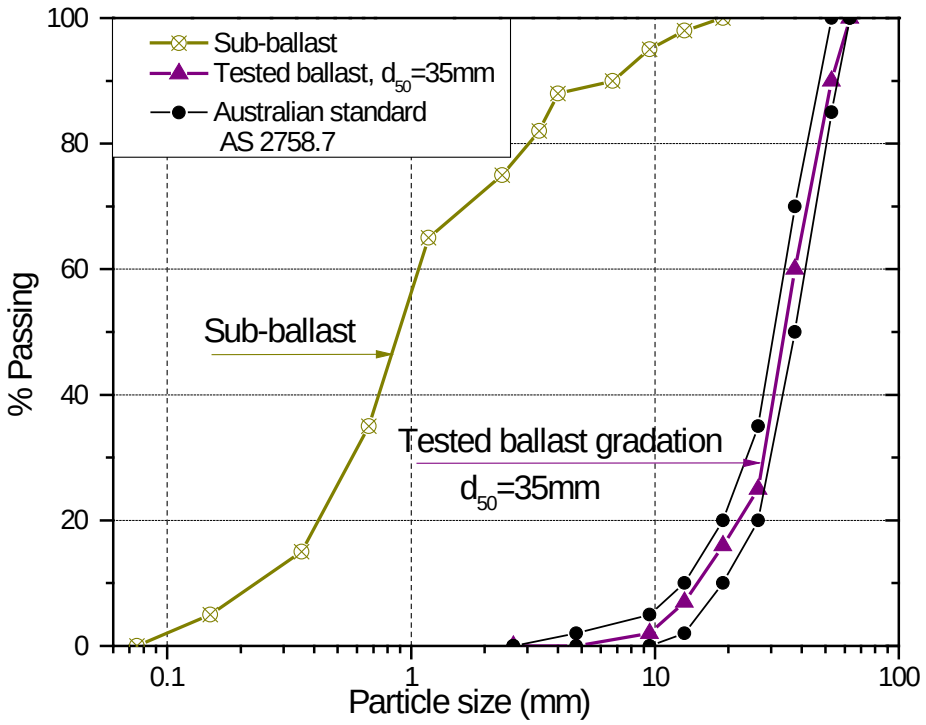

623

624 Figure 2. Particle size distributions of the ballast and capping used in the study

625

(a) Sub-ballast (capping)

(b) Recycled rubber mat tested in laboratory

(c) Clean and dry ballast aggregates

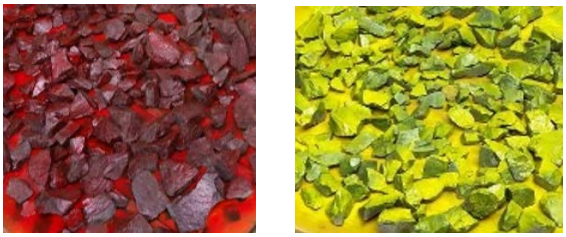

(d) Ballast particles painted in different colours

626 Figure 3. Typical images of capping, ballast particles and recycled rubber mat (READS) used in
627 the laboratory

628

(a) Rubber cell membrane (7 mm thick)

(b) Steel mould surrounding cell membrane

(c) Compacted bottom layer of ballast

(d) Compacted top layer of ballast

(e) Ballast sample before testing

(f) Deformed ballast sample after testing

629 Figure 4. Sample preparation: (a) cell membrane; (b) steel mould, (c) ballast at bottom layer; (c)
630 ballast on top layer; (d) ballast specimen; and (f) deformed shape of ballast specimen

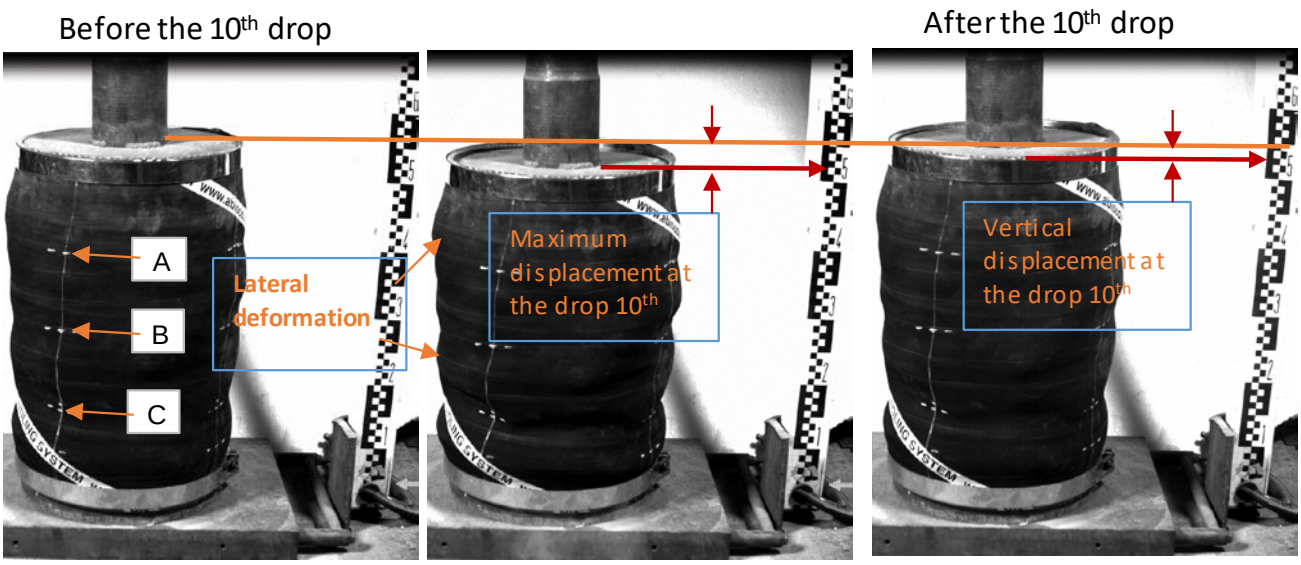

631

632 Figure 5. Typical images of the deformed ballast assembly recorded before and after the 10th
633 drop, taken by the high-speed camera

634

635

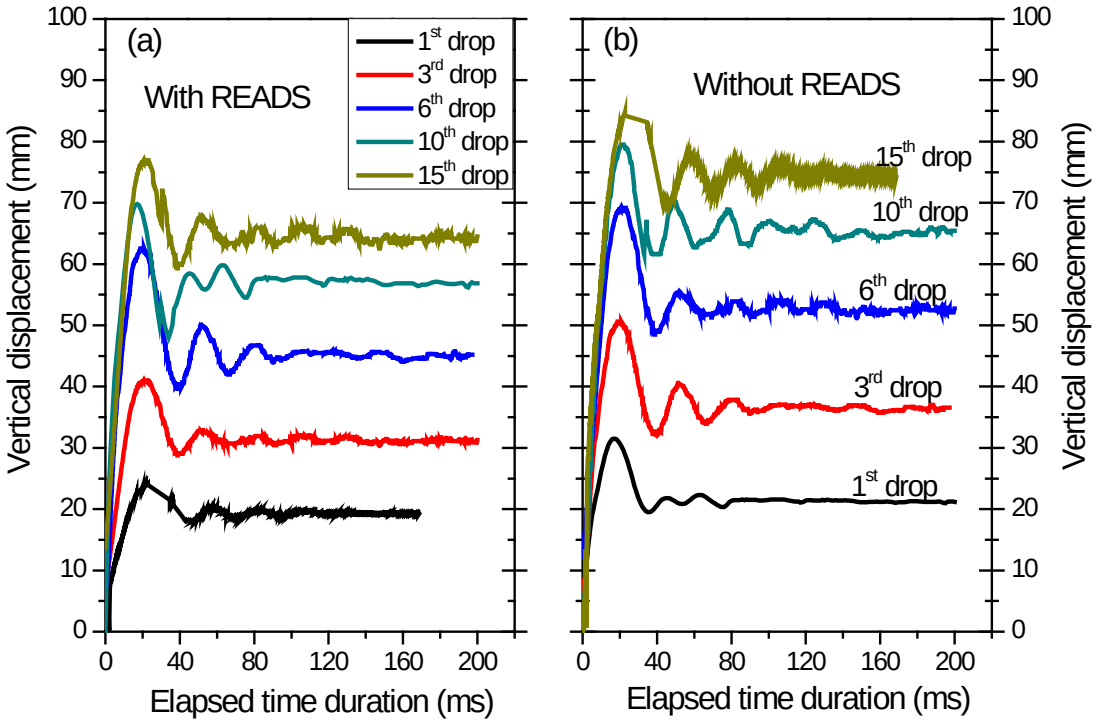

636

637 Figure 6. Measured vertical displacement of ballast assemblies at different drops placed over stiff
638 subgrade: (a) with READS; (b) without READS

639

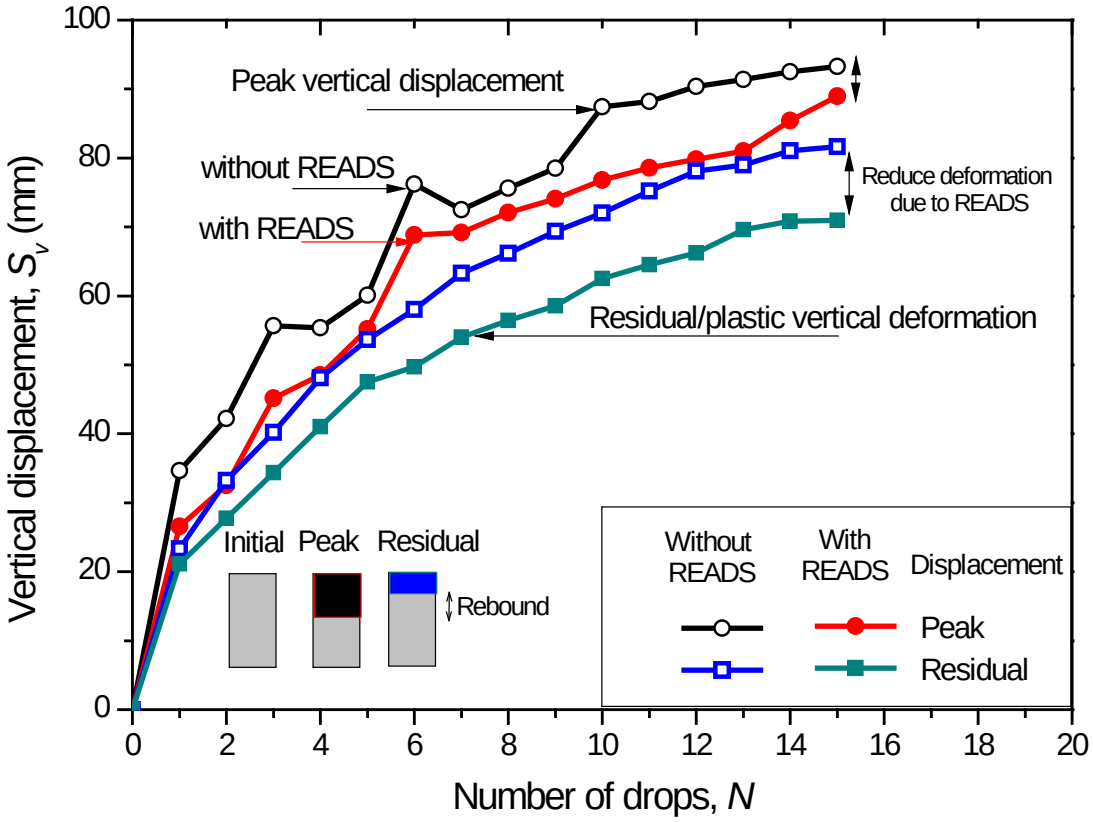

Figure 7. Variation of the peak and residual (permanent) vertical displacement of ballast assemblies with the number of drops

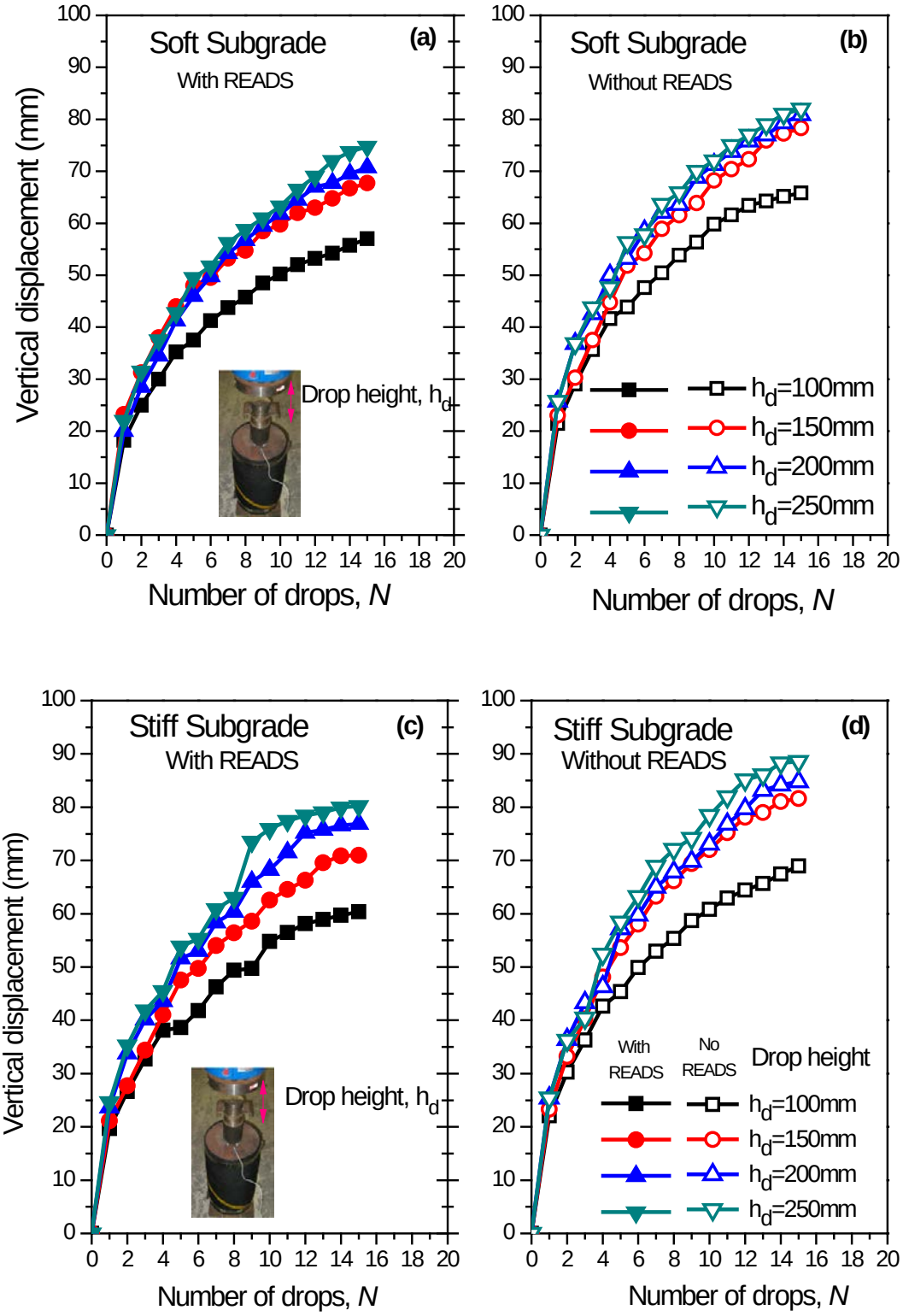

Figure 8. Accumulated permanent vertical settlement of ballast with and without READS: (a)-(b) soft subgrade; (c)-(d): stiff (concrete) base

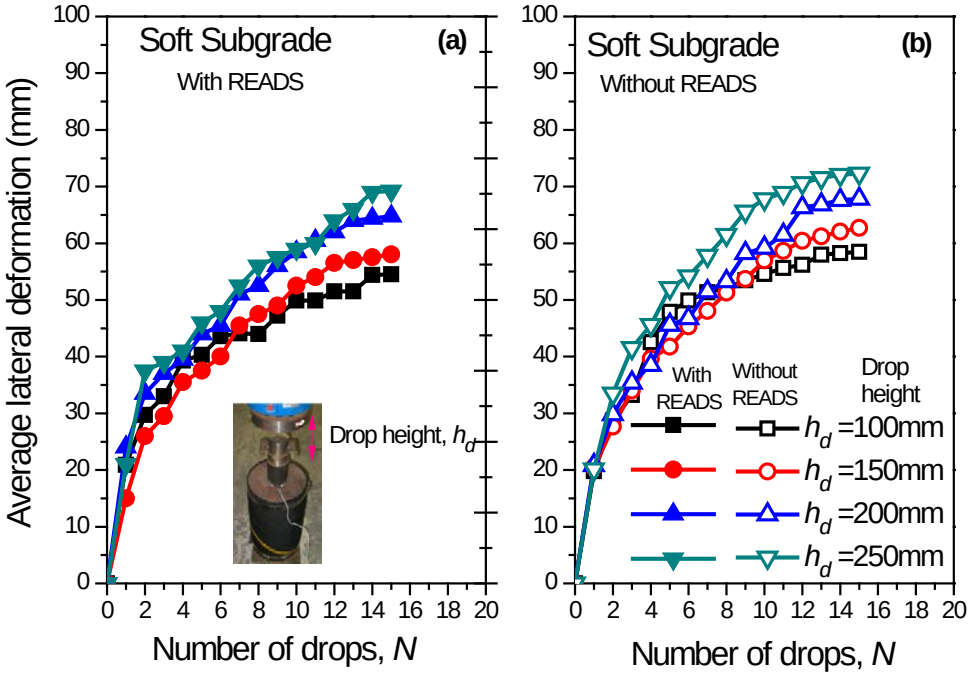

659

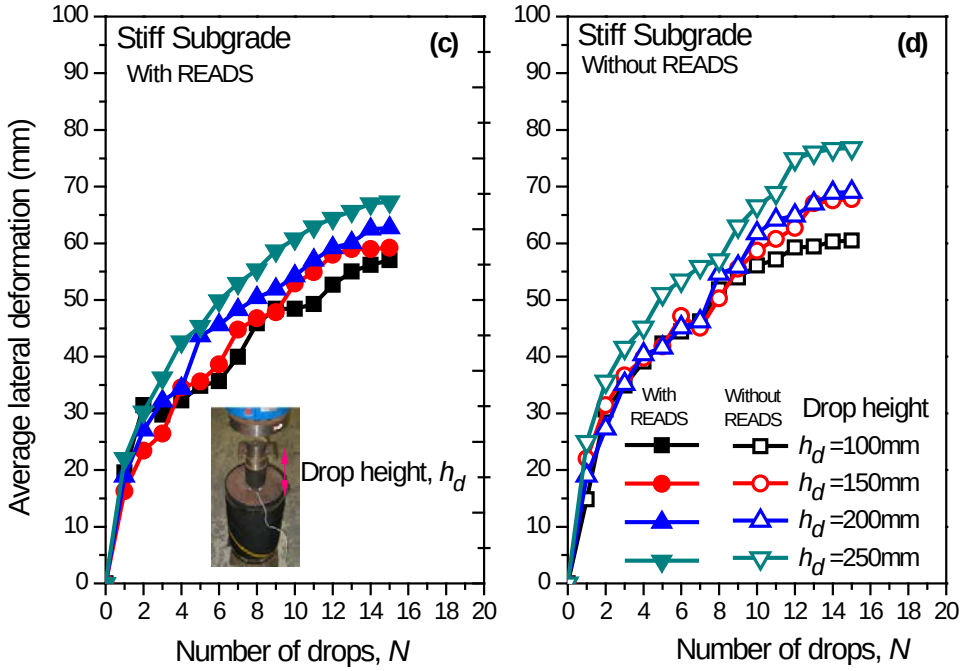

660

661 Figure 9. Average lateral displacement of ballast with and without READS: (a)-(b) soft
662 subgrade; (c)-(d): stiff (concrete) base

663

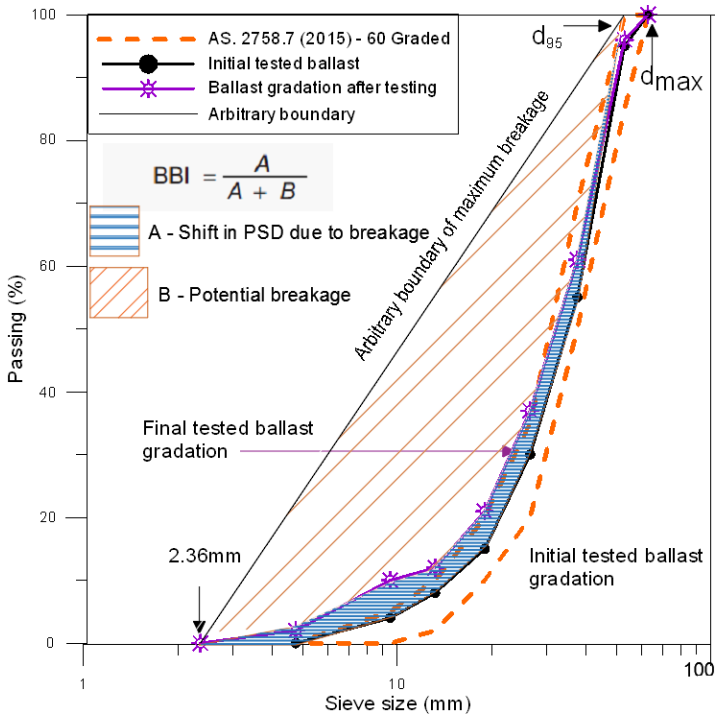

664

665 Figure 10. Quantification of ballast breakage using the ballast breakage index, *BBI*

666

667

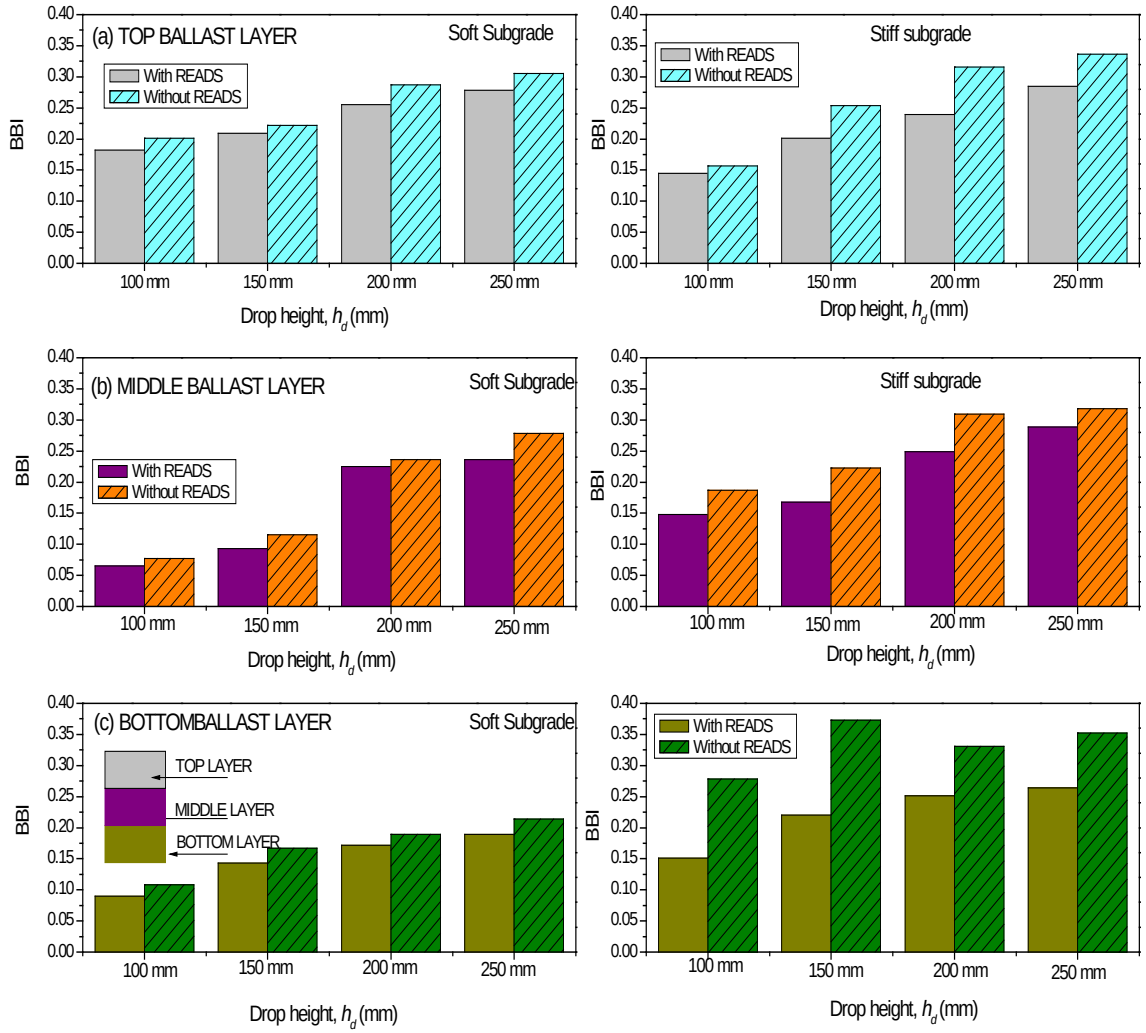

668

669 Figure 11. Ballast breakage index (BBI) for soft and stiff subgrades at different ballast layers
670 subject to varying drop heights: (a) top layer; (b) middle layer; and (c) bottom layer

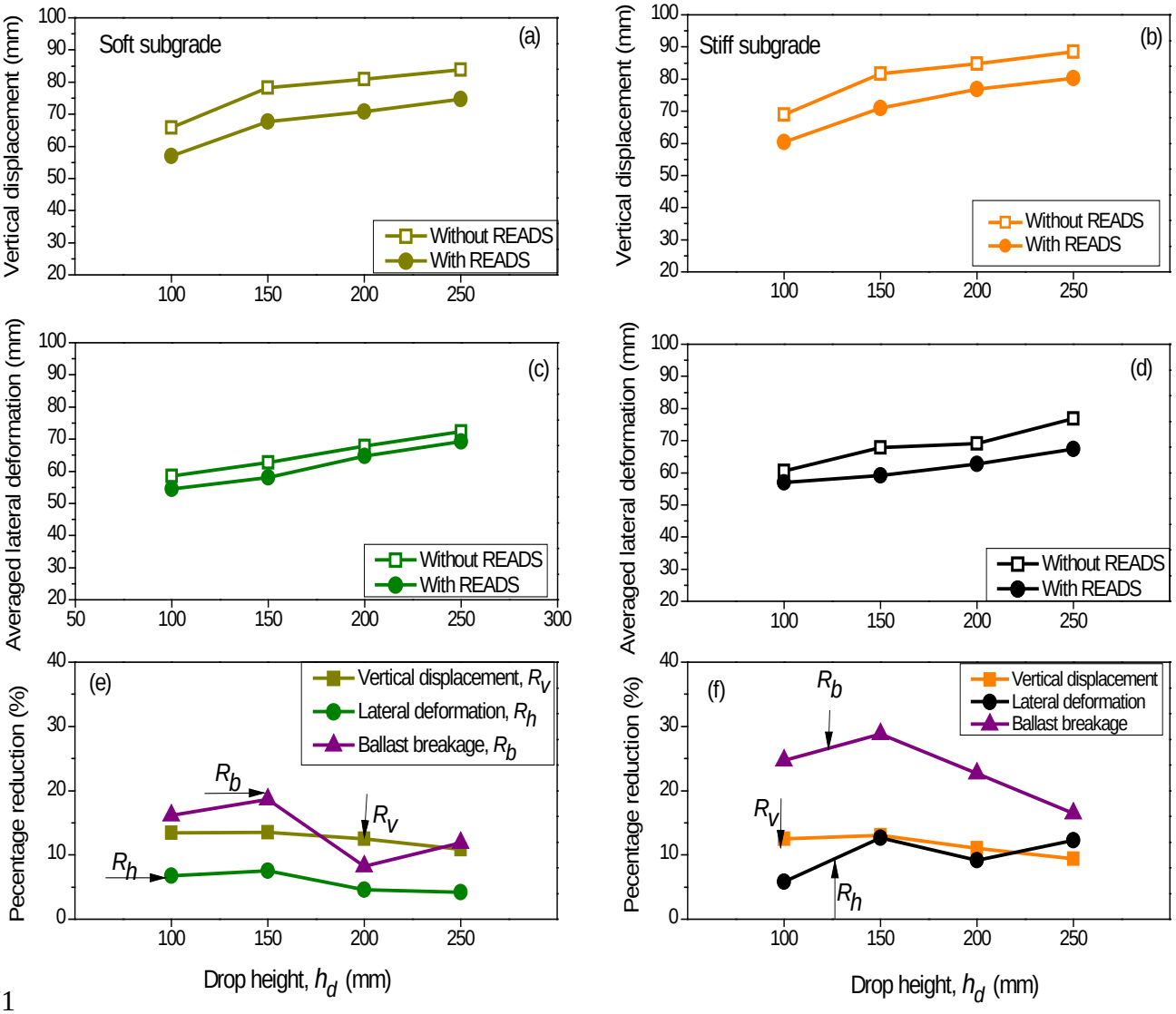

671

672 Figure 12. Variation of final vertical and lateral deformation of ballast placed on soft and stiff
673 subgrades with and without READS at varied h_d: (a-b) vertical displacement; (c-d) lateral
674 displacement; (e-f) percentage reduction of ballast deformation and breakage

675

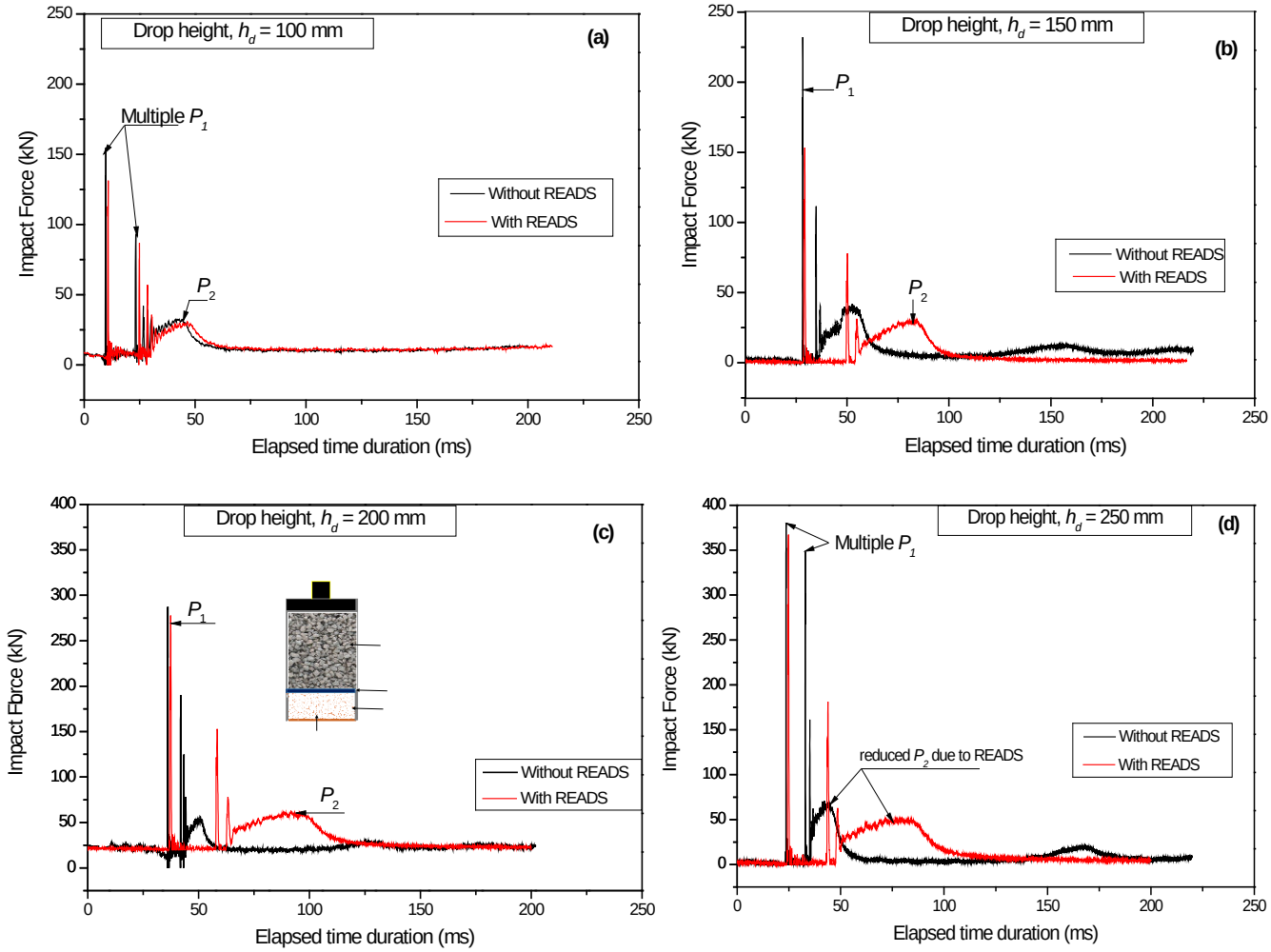

Figure 13. Typical impact force responses of ballast with and without READS placed on soft subgrade measured at the drop N=10, under varying drop heights: (a) h_d=100 mm; (b) h_d =150 mm; (c) h_d =200 mm; and (d) h_d =250 mm.

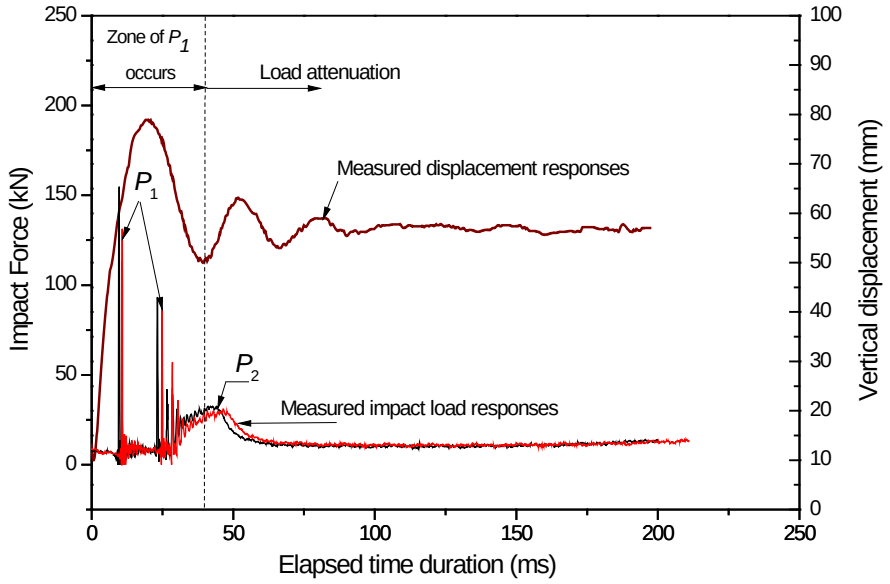

682

683 Figure 14. Measured impact load and vertical displacement of ballast subjected to h_d=100mm

684

685

686

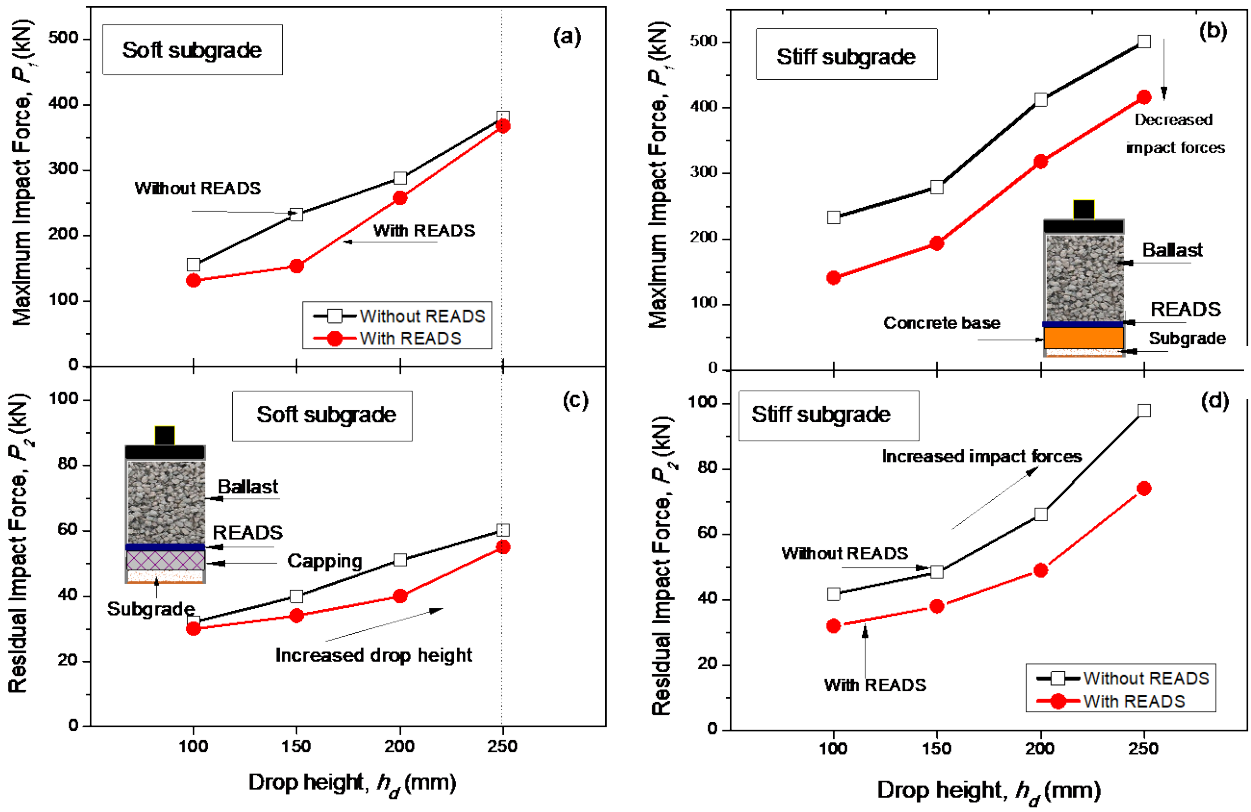

687

688 Figure 15. Measured impact forces, P_1, P_2 for ballast with and without READS under soft and
689 stiff subgrades after 15 drops (N=15): (a) P_1 - soft subgrade; (b) P_1 - stiff subgrade; (c) P_2 – soft
690 subgrade; and (d) P_2 – stiff subgrade

691

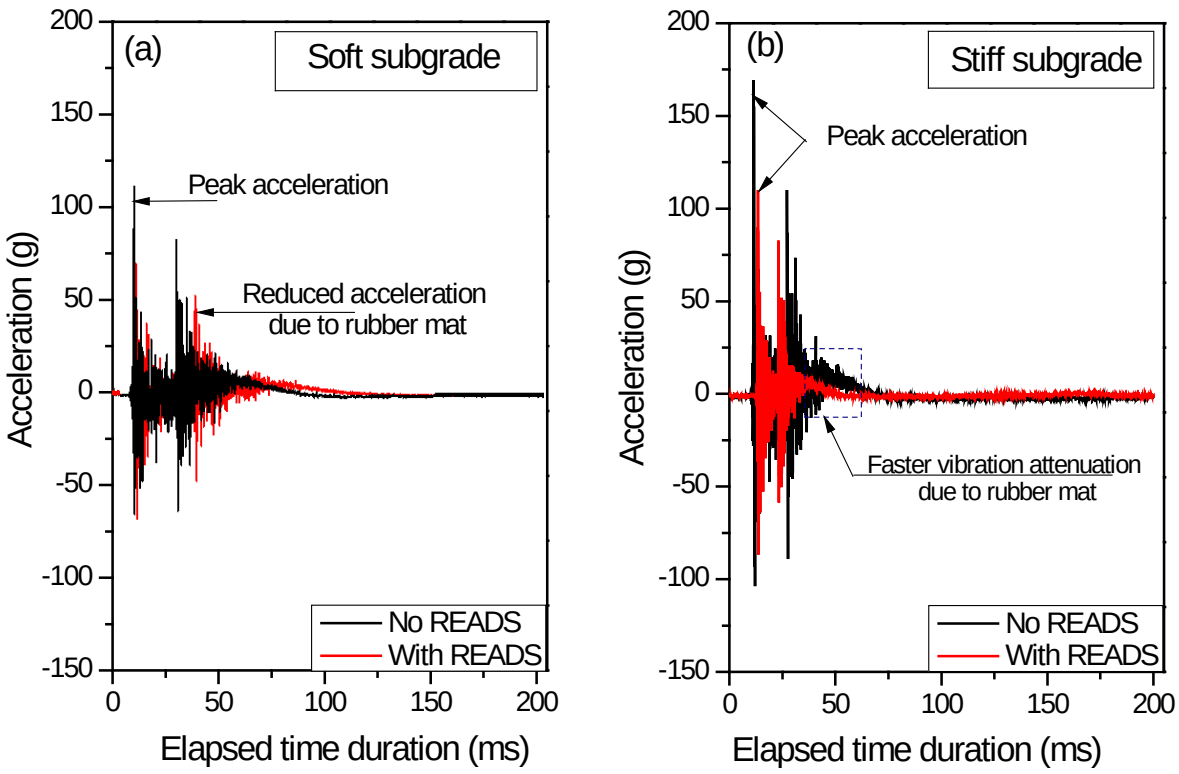

692

693 Figure 16. Measured acceleration of ballast under a drop height of h_d = 100 mm, at the 10th drop

694 (N=10) placed on: (a) soft subgrade; and (b) stiff subgrade

695

696

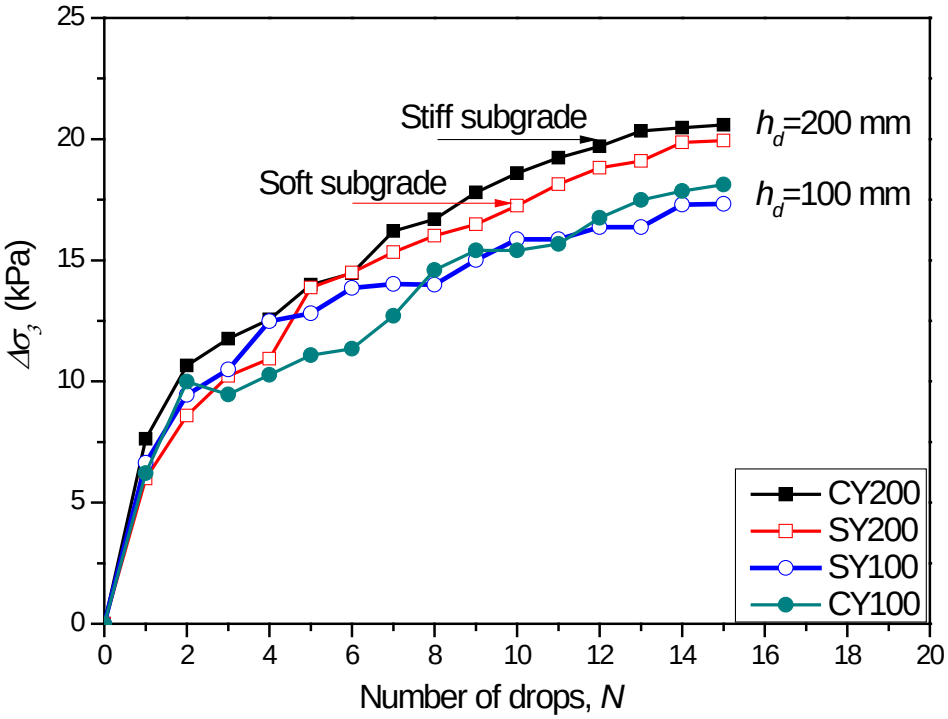

Figure 17. Lateral confining stress applied by the membrane during the loading

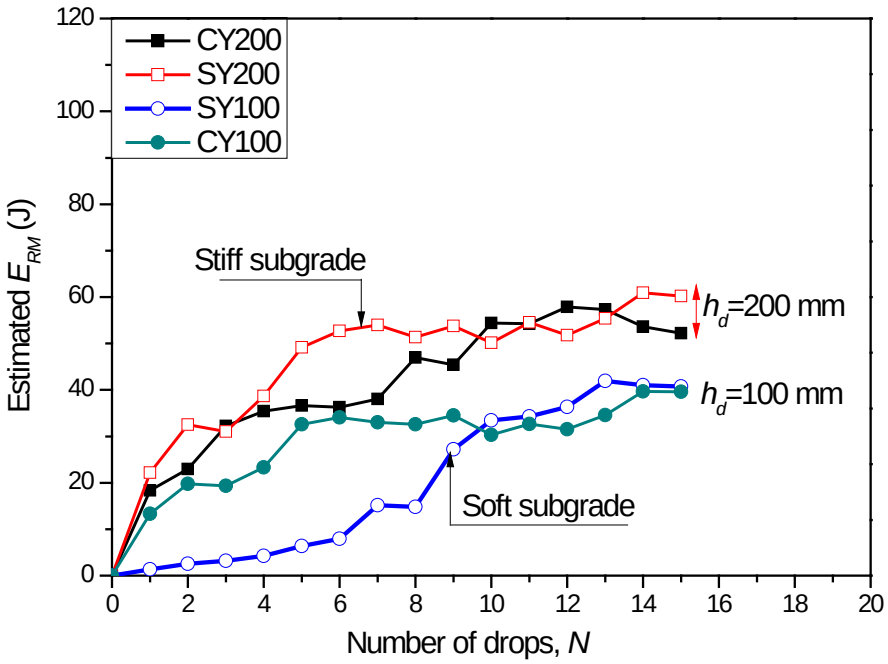

709

710 Figure 18. Estimated energy absorbing of recycled rubber mat (E_{RM}) that is placed on the soft and
711 stiff subgrade materials

712